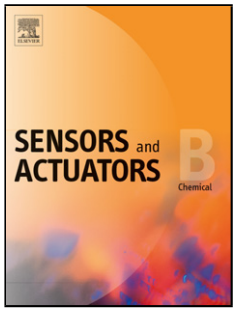

Title: Dense $LaSrMnO_3$ composite electrodes for NO_x Sensing

Authors: N. Pal, E.P. Murray

PII: S0925-4005(17)31894-4
DOI: https://doi.org/10.1016/j.snb.2017.10.014
Reference: SNB 23318

To appear in: *Sensors and Actuators B*

Received date: 27-4-2017
Revised date: 18-8-2017
Accepted date: 3-10-2017

Please cite this article as: N.Pal, E.P.Murray, Dense LaSrMnO3 composite electrodes for NOx Sensing, Sensors and Actuators B: Chemical https://doi.org/10.1016/j.snb.2017.10.014

Dense $LaSrMnO_3$ composite electrodes for NO_x Sensing

N. Pal and E. P. Murray

Institute for Micromanufacturing, Louisiana Tech University, Ruston, Louisiana 71272, USA

Highlights:

- LSM-Au composite sensing electrodes are highly sensitivity to NO_x at low concentrations (i.e., < 50 ppm NO_x) and demonstrate limited cross-sensitivity to H_2O, compared to the LSM and LSM-YSZ electrodes.
- Impedancemetric sensor operation at 20 Hz enabled the maximum NO_x sensing response to be achieved at 575 °C for the LSM based sensors.
- Oxygen cross-sensitivity observed for each of the LSM based sensors can potentially be managed by monitoring the sensor response at frequencies over 5 kHz.
- The response and recovery times for the LSM-Au sensing electrodes may potentially be improved by optimizing the size of the Au particles.
- Improving oxygen reduction reaction steps may further aid the NO_x sensing behavior of LSM-Au electrodes.
- Cross-sensitivity analysis indicated the LSM-Au based sensors were more selective to NO_x, in comparison to CO, CO_2 and CH_4.

I. Introduction

NO_x sensors play a crucial role in monitoring diesel exhaust gases and in communicating with the on-board diagnostic system of a vehicle to regulate engine operation. Typically, such sensors contain a porous platinum (Pt) sensing electrode accompanied by a dense zirconia-based electrolyte. Pt is beneficial as it tolerates the stringent exhaust gas environment, and the porous microstructure of the Pt electrode allows the exhaust gases to diffuse to reactions sites where NO_x sensing occurs. However, Pt is also a strong catalyst for oxygen reduction, which can interfere with accurately detecting NO_x at concentrations below 100 ppm [1,2]. This limitation is

driving research for alternative electrodes for NO_x sensing as advancements in diesel engine technology are resulting in lower NO_x emissions.

Several studies have found metal oxide electrodes, especially those with the perovskite structure (ABO_3), are promising alternative NO_x sensing electrodes as they demonstrate significant sensitivity to NO_x even with high concentrations of oxygen present [1,3–8]. Perovskite electrodes are also attractive as a lower cost alternative to Pt electrodes. Studies on various electrodes have shown substantial NO_x sensitivity at sensors with $LaSrMnO_3$ type perovskite electrodes [1,5–7]. For instance, amperometric NO_x sensor studies with electrodes composed of $La_{0.8}Sr_{0.2}MnO_3$ reported greater sensitivity to NO_2 over a concentration range of 50 – 800 ppm, in comparison to other lanthanum-based electrodes, as Sr enhanced the sensor response [7]. In potentiometric NO_x sensor studies, $(La_{0.8}Sr_{0.2})_{0.95}MnO_3$ sensing electrodes were reported to detect NO_2 at concentrations of 40 – 1000 ppm with greater sensitivity and more rapid response/recovery rates than sensors using Pt sensing electrodes [6]. NO_x sensitivity at concentrations as low as 5 ppm has been achieved using dense $(La_{0.85}Sr_{0.15})_{0.98}MnO_3$ sensing electrodes in impedancemetric sensor studies [5]. The dense electrode microstructure apparently limits heterogeneous catalysis reactions that can limit NO_x sensitivity at low concentrations [1,8,9]. In addition, impedancemetric operation has been noted for promoting greater sensor accuracy and stability [1]. $LaSrMnO_3$ sensing electrodes have also demonstrated low cross-sensitivity to NH_3, CO and hydrocarbons [6,7,10]. However, the beneficial sensing properties of $LaSrMnO_3$ electrodes are accompanied by cross-sensitivity to water and oxygen that limit sensor accuracy [10].

An effective approach for enhancing gas sensor sensitivity and selectivity is adding another component to the sensing electrode to form a composite, according to numerous studies

described in recent review articles by Miura et al. and Liu et al. [11,12]. Desired sensing properties can be tailored by varying the material composition and microstructure of the electrode, which affect the electrochemical response of the sensor. Numerous composite electrodes have been studied for enhanced sensitivity and selectivity for CO, CO_2, NH_3 and hydrocarbon sensors [13–17]. There have also been some studies that have explored the potential of composite electrodes for NO_x sensing. For example, potentiometric NO_x sensors using Cr_2O_3-WO_3 sensing electrodes demonstrated greater sensitivity to NO_2 along with a more rapid response time, in comparison to WO_3 sensing electrodes [18]. Similar results were reported for Au-YSZ composite sensing electrodes where impedance data indicated the addition of 10 wt% YSZ to the Au electrode enhanced the electrochemical response of the sensor to NO_2 [19]. Perovskite composites have been used as catalysts for propane oxidation at solid oxide fuel cells [20]; however, there appear to be limited studies concerning perovskite composite electrodes with respect to NO_x sensing [21]. Impedance characterization studies on $La_{1-x}Sr_xMnO_3$ electrodes containing praseodymium- or gadolinium-doped ceria under NO_x gas environments suggest the ionic and electronic properties of the electrode can be modified to influence electrode reactions [22]. Thus, further study of perovskite composites for NO_x sensing can potentially provide insight for limiting undesirable reactions, such as water and oxygen cross-sensitivity, as well as offer additional knowledge regarding the role of electrode composition on reactions that influence NO_x gas sensing.

In the present study, NO_x sensors composed of sensing electrodes containing $LaSrMnO_3$ and Au or Y_2O_3-ZrO_2 with dense microstructures were operated using the impedancemetric method. Au was chosen as several studies have reported high NO_x sensitivity with low water cross-sensitivity for sensors using dense Au electrodes [10,23]. In addition, gas sensor studies

with composite electrodes containing up to 10 wt% Au have reported stable microstructural and electrical performance over several hours of operation [11,24]. $LaSrMnO_3$-Au sensing electrodes are also expected to be more compatible with typical high temperature sensor firing processes, in comparison to pure Au electrodes due to the low melting temperature of Au. The sensors based on the $LaSrMnO_3$ – Y_2O_3-ZrO_2 composite electrode contained pathways for oxygen ion transport due to the addition of Y_2O_3-ZrO_2. Oxygen ions are known to participate in interfacial gas reactions and can interact with water reactions resulting in hydroxyl groups that can effect reactions involving NO_x [1,25]. Both types of composite electrodes were accompanied by a Y_2O_3-ZrO_2 porous electrolyte that enabled gas diffusion to the electrode/electrolyte interface. The impedancemetric NO_x sensors using $LaSrMnO_3$-Au and $LaSrMnO_3$ – Y_2O_3-ZrO_2 composite sensing electrodes were investigated under dry and humidified gas conditions. The electrochemical response, gas cross-sensitivity, response time, and rate-limiting mechanisms of the sensors are discussed.

2. Experimental

Powders of $La_{0.8}Sr_{0.2}MnO_3$ (LSM, Inframat Advanced Materials), 8 mol% Y_2O_3-doped ZrO_2 (YSZ, Tosoh Corporation) and Au (Alfa Aesar) were used to fabricate 3 types of NO_x sensors based on the following electrode supports: LSM, LSM-Au, and LSM-YSZ. The LSM based sensors were used for comparison purposes. The LSM-Au and LSM-YSZ composite electrodes contained 10 wt% Au and 30 wt% YSZ, respectively. The powders for each electrode were ball milled with 3 wt% polyvinyl buteral (B-76, Butvar) binder and ethanol for approximately 16 hours. The resulting slurry was dried and uni-axially pressed at 200 MPa into pellets. The LSM and LSM-Au pellets were fired at 1400 °C for 5 hours where the ramp rate was 4 °C/min. The LSM-YSZ pellets were fired at 1325 °C for 6 hours with a ramp rate was 4

°C/min. The lower temperature was used to avoid reactions between the LSM and YSZ powders. The electrode pellets were partially coated with a YSZ electrolyte slurry. The YSZ slurry contained 8 mol% Y_2O_3-doped ZrO_2 powder along with the following additives: 2 wt % B-76 Butvar binder, 2 ml phosphate ester dispersant along with ethanol and was ball milled for 12 hours. The YSZ coated pellets were fired at 1000 °C for 1 hour using a ramp rate of 2 °C/min. The sensors were completed by applying a counter electrode made from a slurry containing LSM, LSM-Au, or LSM-YSZ. The counter electrode slurries consisted of the desired electrode powder along with 2 wt % B-76 Butvar binder, 2 ml corn oil dispersant with methyl ethyl ketone solvent and ball milled for 22 hours. A final firing step at 1000 °C for 1 hour at a ramp rate of 2 °C/min completed sensor fabrication. The resulting sensors were supported by a dense electrode pellet with a porous electrolyte and porous counter electrode as shown in the diagram of Fig. 1. The diameter of the pellet was 11 mm with a thickness of about 1.1 mm after firing. Scanning electron microscopy (SEM), energy dispersive x-ray (EDX) and x-ray diffraction (XRD) was used to analyze the morphology and microstructure of the sensor components.

Electrochemical impedance measurements were collected using a Gamry Reference 600 (Gamry Instruments) for sensors operating at temperatures ranging from 575 – 675 °C. Measurements were performed within a quartz tube that was placed inside of a furnace. The sensors were exposed to NO and NO_2 at concentrations ranging from 0 - 100 ppm for dry and humidified gas (10% water vapor) environments. The water vapor was introduced to the system by using a bubbler along with heated gas lines. The test exhaust gas also contained O_2 at concentrations of 5% - 18% with N_2 as a balance. A standard gas handling system with mass flow controllers was used to regulate and vary the gas concentrations where the total flow rate was 500 sccm. Impedance spectroscopy data was collected using a signal amplitude of 100 mV

over a frequency range of 1 Hz - 1 MHz. Measurements were collected in triplicate to insure stable and reproducible data was collected.

3. Results and discussion

3.1 Morphology and Microstructure

Typical SEM images of the electrode pellets and electrolyte for the sensors are shown in Fig. 2. Clearly observable grains and grain boundaries were seen over the surface of the LSM, LSM-Au and LSM-YSZ dense pellets (see Fig. 2a, 2b, and 2c). The grain sizes within the LSM and LSM-Au electrode pellets ranged from about 5 µm to almost 20 µm. The backscattered SEM image of the LSM-Au pellet indicated the Au particles were well dispersed. Fig. 2c shows the surface of the LSM-YSZ composite pellet. EDX results indicated the dark phases were YSZ and the lighter phases were LSM. XRD analysis confirmed no resistive phases formed within the LSM-YSZ composite electrodes. Some pores were observed over the LSM-YSZ surface, and the grains appeared to be smaller than those composing the LSM and LSM-Au electrode pellets. The density of the sensing electrode pellets without the YSZ coating was determined by Archimedes method to be about 93% ± 2%. Comparable results measured by mercury intrusion porosimetry indicated the pellets were 91% ± 3% dense. SEM surface images of the YSZ coating indicated a contiguous network of particles and dispersed pores as shown in Fig. 2d. The electrolyte porosity was estimated to be approximately 48% based on computational analysis of similarly prepared YSZ electrolyte coatings [26]. The YSZ coating was determined to have a thickness of ~0.2 mm.

3.2 Impedance Response

Impedance measurements were collected for the LSM, LSM-Au and LSM-YSZ based NO_x sensors for various gas concentrations during operation at temperatures ranging from 575 -

675 °C. In Fig. 3 the real, Z', and imaginary, Z'', impedance is plotted for sensors based on the three types of sensing electrodes for operation at 575 °C in 10.5% O_2 and with the addition of 100 ppm NO and 10% H_2O where N_2 was the balance gas. Two distinct frequency ranges were observed for each of the sensors. The impedance response at higher frequencies described temperature dependent reactions occurring at the YSZ electrolyte. These reactions were related to the YSZ electrolyte ionic conductivity and porous microstructure [26,27]. The lower frequency impedance response was used to interpret NO_x behavior as the distorted arc varied with gas concentration, as well as temperature. The data at lower frequencies represented reactions occurring at the electrode and electrode/electrolyte interface. For each sensor type the impedance arc for lower frequencies decreased when NO was added to the test gas. The impedance response for sensors operating with NO_2 was comparable to that for NO. Such findings have been observed in other studies for sensors operating under similar conditions and attributed to a predominant amount of NO_2 undergoing thermodynamic conversion to NO [26,28]. Therefore, the work presented here concentrates on the behavior of the sensors in the presence of NO. As the operating temperature of the sensors decreased the impedance increased. Also, the impact of the gas concentration on the sensor impedance response became more noticeable with decreasing operating temperatures. Therefore, data collected at the lowest operating temperature of 575 °C was more useful for assessing the response of the sensors to changes in gas composition.

The measured impedance was lower for humidified gas conditions, in comparison to dry gas conditions for each of the sensors evaluated. This is illustrated in the data shown in Fig. 3 where in each case the addition of 10% H_2O to the gas stream containing 10.5% O_2 and 100 ppm NO resulted in an impedance that was smaller than the dry gas measurements with oxygen and

NO. Water vapor is understood to form hydroxyl groups at perovskite and YSZ surfaces [29,30]. The addition of water vapor may facilitate the charge transfer process at the triple phase boundary, which can reduce the impedance [25]. The triple phase boundary (TPB) is the location where the electrode, electrolyte and gas phases meet. It is possible that water reactions at sensors with LSM-YSZ electrodes (see Fig. 3c) resulted in a greater coverage of adsorbed species at the TPB as the impedance changed more substantially for these sensors under humidified versus dry gas conditions with NO.

The sensors with an LSM electrode had a lower impedance than sensors with an LSM composite electrode. The differences in the magnitude and profile of the impedance data were indicative of the different electrode resistances and interfacial reactions taking place at the LSM, LSM-Au and LSM-YSZ based sensors. Reactions commonly associated with NO_x sensing are given by the following equations [31]:

$$\frac{1}{2}\,O^{2-} + 2e^{-} \leftrightarrow\ O^{2-} \qquad (1)$$

$$NO + \ O^{2-} \leftrightarrow NO_2 + 2e^{-} \qquad (2)$$

$$NO_2 \leftrightarrow NO + \frac{1}{2}O^2 \qquad (3)$$

The electronic and ionic conductivity of the sensing electrode, as well as the porosity of the electrolyte, influenced how readily these reactions were able to proceed. Unfortunately, the impedance response does not provide clear distinction of dominant reactions. Therefore, it is not certain which of these or other reactions proceeded more readily.

Equivalent circuit modeling was used to further interpret the electrical response of the LSM and LSM composite based NO_x sensors. As shown in Fig. 4, two parallel circuits were

found to model the impedance response of each sensor for various operating conditions where the data at high and low frequencies were described by R_{HF}CPE and R_{LF}(CW) circuits, respectively. The errors associated with the equivalent circuit model were between 1 – 2%. The resistance, R_{HF}, was associated with high frequency reactions taking place within the porous YSZ electrolyte; and, the constant phase element, CPE, related to non-ideal capacitance behavior. At 575 °C, the best-fit values for R_{HF} for the 3 types of sensors were between 4.9 kΩ – 5.6 kΩ. The narrow range for R_{HF} was likely due to the sensors having a YSZ electrolyte with comparable porosity and thickness, thereby, resulting in similar electrolyte reactions. The impedance, Z_{CPE}, due to the CPE is defined by $Z_{CPE} = [Y_o(j\omega)]^{-n}$, where n is a constant, such that $n = 1$ describes a pure capacitor with a value of Y_o. The angular frequency is $\omega = 2\pi f$, and f is the applied operating frequency. The equivalent circuit model indicated $n \approx 0.85$ for the various sensors evaluated, suggesting that the high frequency response resembled nearly ideal capacitance behavior. In the second parallel circuit, R_{LF} was associated with the low frequency resistance of the sensing electrode and electrode/electrolyte interfacial reactions. The calculated R_{LF} values were used to assess rate-limiting mechanisms discussed in a latter section. The lower frequency circuit also included a capacitor, C, and Warburg impedance, W. The capacitance associated with the LSM and LSM-Au based sensors during operation at 575 °C was approximately 1.30 μF and 0.75 μF, respectively, and did not vary significantly with changes in O_2, NO, or H_2O. However, the capacitance of the LSM-YSZ based sensors operating at the same temperature decreased from ~2.5 μF to ~1.5 μF when the O_2 concentration increased from 5 – 18%, and remained close to 1.5 μF with the addition of NO and H_2O to the gas stream. The Warburg element described the impedance resulting from diffusion of ionic species at the electrode/electrolyte interface [32]. The Warburg element was about 5.7×10^{-6} $S*s^{1/2}$ and

increased by approximately 2% with increasing O_2 concentrations. No significant changes were observed for the Warburg element as the NO concentration varied for the LSM and LSM composite based sensors evaluated. The value of the Warburg element increased ~5% due to water addition to the test environment.

3.3 Angular Phase Response

NO_x sensor studies report that the angular phase response indicates changes in gas concentration with greater sensitivity and accuracy, in comparison to measuring the magnitude, $|Z|$, or other components of the impedance [1]. The angular phase response, θ, is defined according to the following equation:

$$\theta = tan^{-1}\frac{Z''(\omega)}{Z'(\omega)}. \qquad (4)$$

Fig. 5 shows the phase angle response versus the operating frequency for sensors operating with and without 100 ppm NO and with the addition of 10% H_2O at 575 °C. Sensors with the LSM-Au sensing electrode achieved the highest phase angle peak response of -19.6° with 10.5% O_2 and N_2 as shown in Fig. 5b; whereas, the lowest peak phase angle response of -13.3° was demonstrated by LSM-YSZ based sensors under similar conditions given in Fig. 5c. Operation with 10.5% O_2 and N_2 as the balance represented baseline gas conditions. The addition of 100 ppm NO caused the peak phase angle to decrease for all sensors. This decrease was more substantial in sensors with the LSM-Au sensing electrode. This data suggested that the LSM-Au sensing electrode can enable a larger signal and greater response to NO, in comparison to LSM and LSM-YSZ sensing electrodes. The θ versus frequency curves for 100 ppm NO with O_2 and N_2 merged with the baseline gas data at about 90, 125, and 250 Hz for the sensors composed of LSM-YSZ, LSM and LSM-Au electrodes, respectively. So, the LSM-Au based sensors can

potentially enable impedancemetric operation over a wider range of frequencies, which can be beneficial for optimizing sensor performance. Adding 10% H_2O to the gas stream caused a further decrease in the θ versus frequency response for the sensors. There was a strong overlap in the dry and humidified data with 100 ppm NO for the sensors with the LSM-Au electrode for frequencies up to ~50 Hz, as seen in Figure 5b. This overlap in the data indicated the range of frequencies where the LSM-Au based sensors could avoid cross-sensitivity to water while detecting NO. There was little overlap at lower frequencies for the dry and humidified frequency curves for the LSM and LSM-YSZ based sensors. At much higher frequencies (i.e., > 5 kHz) the response to NO and H_2O merged with the baseline gas response for each of the sensors. It has been suggested that measuring the sensors response at higher frequencies can be a method for separating the detection of O_2 from NO_x, since the baseline gas condition describes the sensor response to O_2 [1]. This approach would provide a means for managing O_2 cross-sensitivity.

3.4 NO Sensitivity

The sensitivity to NO for the LSM and LSM composite electrode sensors was based on the change in the angular phase response, $\Delta\theta$, for various NO concentrations according to the following:

$$NO\ sensitivity = \frac{\Delta\theta}{[\Delta NO]}\ \ (degrees/ppm) \qquad (5)$$

where $\Delta\theta = \theta_{O2} - \theta_{NO}$. The terms θ_{O2} and θ_{NO} were the angular phase response for 10.5% O_2 and N_2, and with a specific amount NO added, respectively. The largest $\Delta\theta$ values occurred at 20 Hz according to the θ versus frequency data plotted in Fig. 5. Thus, the maximum sensor sensitivity to NO was based on sensor operation at 20 Hz. Fig. 6a shows the NO sensitivity of LSM, LSM-Au and LSM-YSZ based sensors under dry operating conditions. A high and low sensitivity

range was observed for each sensor type where higher sensitivities were calculated for lower NO concentrations (i.e., ≤ 50 ppm). Similar behavior has been reported in other impedancemetric NO_x sensor studies [33]. For dry gas conditions, the highest sensitivity of 0.051 deg/ppm NO was demonstrated by sensors with an LSM-Au electrode for operation at 575 °C. For comparable operating conditions, the LSM-Au based sensors were ~25% more sensitive to NO than the LSM based sensors and ~50% more sensitive than LSM-YSZ based sensors. Since NO_x sensors composed of a pure Au sensing electrode and YSZ electrolyte have achieved a gas sensitivities of ~0.07 deg/ppm NO [5], it is likely that the Au addition to the LSM enhanced the sensing response of the LSM-Au electrode. As for the sensors with the LSM-YSZ electrodes, it is possible that the YSZ addition reduced the TPB length such that NO_x sensing reactions were limited. The TPB was determined according to sites where the gas phase was in contact with LSM and YSZ particles. The YSZ addition to the sensing electrode reduced the placement of LSM particles along the electrode/electrolyte interface, thereby, limiting the TPB length. Adding water to the gas stream caused a slight increase (~ 7%) in NO sensitivity for LSM-Au based sensors, as shown in Fig. 6b. Optimizing the Au concentration within the LSM-Au sensing electrode may reduce the difference between the dry and humidified sensing response to NO. Substantially larger increases in NO sensitivity were observed for the LSM and LSM-YSZ based sensors as the humidified gas caused a 20 – 30% higher sensing response.

3.5 Sensor Response Rates

The response time of the LSM, LSM-Au and LSM-YSZ based sensors was evaluated by measuring the change in the angular phase angle over time. Fig. 7 shows time based data of the sensors for baseline conditions with 10.5% O_2 and N_2 along with 5, 10, and 25 ppm NO for an

operating frequency of 20 Hz at 575 °C. The LSM and LSM-YSZ based sensors had an average response time, τ_{90}, of 15 and 17 seconds, respectively; whereas, LSM-Au based sensors were slower as τ_{90} was 20 seconds based on data collected at 5 ppm NO. The recovery time for LSM-Au and LSM based sensors to return to baseline conditions was ~35 seconds; and, the LSM-YSZ based sensors had a slightly faster recovery of about 30 seconds. The recovery time of the sensors was possibly related to the adsorption of NO at the electrode [19]. In other sensor studies using composite $ZrCr_2O_4$-Au electrodes it was found that the response and recovery time of the sensors was dependent upon the size of the Au particles composing the sensing electrode [15]. Thus, it may be possible to improve the LSM-Au sensor response and recovery time by altering the size of the Au particles.

3.6 Rate Limiting Mechanisms

Oxygen reduction reactions at LSM based electrodes are often used to interpret rate limiting reactions at solid oxide fuel cells (SOFCs) [34–36]. Identifying such reactions can be useful for understanding and improving the operation of SOFCs, as well as NO_x sensors. Numerous studies report oxygen reduction at LSM electrodes can take place according to two separate reaction pathways. One reaction pathway proceeds by oxygen diffusion to the TPB resulting in electrochemical oxygen reduction [34]. The other reaction pathway is based upon surface adsorption resulting in oxygen ion transport through the electrode. This reaction pathway is typically limited to thin film LSM electrodes as oxygen ionic conductivity in LSM is low. In the present study, the porous YSZ electrolyte enabled gas diffusion to the TPB, as well as oxygen ion transport through the YSZ particles. The LSM and LSM-Au electrodes primarily supported electron transport. Electrons and oxygen ions were able to travel through the LSM-YSZ composite electrodes. The rate limiting mechanisms associated with the NO_x sensors was

evaluated using the power law relationship, R_{LF} α $(P_{O_2})^m$, where R_{LF} was the low frequency resistance determined from equivalent circuit analysis, P_{O2} represented the oxygen partial pressure, and *m* indicated the rate limiting mechanism(s). Table 1 shows the value of the power law exponent, *m*, for sensors based on LSM, LSM-Au, and LSM-YSZ electrodes for operation under various gas conditions. The LSM and LSM-YSZ based sensors had a weak P_{O2} dependence under dry operating conditions. Adding NO caused a slight reduction in the P_{O2} dependence; whereas, adding H_2O generated a stronger dependence. Similar behavior was observed for the LSM-Au based sensors, although the overall P_{O2} dependence was greater. Other studies have reported that a $(P_{O2})^{-0.25}$ dependence describes the transport of partially reduced atomic oxygen to the TPB [37,38]. In addition, the complete reduction on oxygen at the TPB is represented by a $(P_{O2})^m$ relationship where $m = 0$. Thus, it is possible that under dry conditions the response of the LSM and LSM-YSZ sensing electrodes was limited by a combination of atomic oxygen transport and oxygen reduction. Adding H_2O to the gas stream appeared to improve atomic oxygen transport as the value of *m* was near -0.25 for each of the sensors. The sensing response of the LSM-Au electrodes seemed to be primarily limited by the rate of oxygen reduction at the TPB as *m* was close to -0.25 for the various gas conditions evaluated. Thus, improving oxygen reduction at the LSM-Au/YSZ interface may contribute to a greater NO_x response.

The temperature dependence of the sensors was based on calculations of the activation energy using the R_{LF} values associated with each type of sensor. The activation energies for operating in 10.5% O_2 with N_2 were 1.04, 1.07, and 1.09 eV for sensor with LSM, LSM-YSZ, and LSM-Au, respectively. These values were lower than the activation energies commonly reported for LSM based electrodes. It is possible that the dense electrode microstructure and the

fabrication process contributed to the lower activation energy values that were determined. As expected, adding NO caused a slight decrease in the activation energies. This decrease suggested that NO_x reactions were able to proceed more readily, which is in agreement with the impedance data shown in Fig. 3. The addition of NO could have also interfered with atomic oxygen transport to the TPB as NO may have occupied interfacial sites in place of oxygen. Such a case would support the rate limiting mechanism data presented in Table 1. The activation energies for humidified gas conditions were approximately 1 eV for each of the sensors. This further reduction also agrees with the impedance data. Considering oxygen reduction seemed to be the dominant rate limiting mechanism, it is possible that water aided the NO_x reactions instead of the O_2 reactions.

3.7 NO_x Selectivity of LSM-Au based Sensors

The electrochemical behavior of the LSM-Au based sensors suggests that such sensors may be more suitable for NO_x sensing applications, in comparison to LSM and LSM-YSZ based sensors. To further investigate the feasibility of LSM-Au based sensors selectivity measurements were carried out with 100 ppm NO, NO_2, CO, CO_2 and CH_4 with air as the background gas. Fig. 8 shows the change in the angular phase response with respect to time for LSM-Au based sensors operating at a frequency of 20 Hz at 575 °C. As expected, the NO and NO_2 responses were similar most likely due to thermodynamic conversion as discussed previously. The response of the sensors to CO and CO_2 was substantially lower than that for NO_x gases indicating low cross-sensitivity. Although the LSM-Au based sensors did show a noticeable response to CH_4, the sensitivity to CH_4 was about 70% lower than the sensitivity to NO_x.

4. Conclusions

The impedancemetric NO_x sensing behavior of dense LSM, LSM-Au and LSM-YSZ electrodes were evaluated under dry and humidified gas conditions for a range of operating conditions. The LSM-Au composite electrodes demonstrated the highest response to NO with limited cross-sensitivity to H_2O, in comparison to the LSM and LSM-YSZ electrodes. The angular phase versus the frequency behavior of the sensors indicated the maximum sensing response to NO was achieved at 20 Hz with an operating temperature of 575 °C. Managing oxygen cross-sensitivity could potentially be carried out at by monitoring the sensor response at frequencies over 5 kHz. The response and recovery times for the LSM-Au sensing electrodes were not as rapid as those for LSM and LSM-YSZ, however, altering the Au particle size may improve the performance rate of LSM-Au based sensors. Oxygen reduction appeared to be the dominant rate limiting mechanism for the sensors during operation with humidified gas conditions. For dry gas conditions, transport of atomic oxygen became an additional rate limiting mechanism for the LSM and LSM-YSZ based sensors. The LSM-Au based sensors were highly selective to NO_x, in comparison to CO, CO_2 and CH_4 gases. Overall, the Au addition to LSM appeared to enhance sensor sensitivity to NO by enabling NO_x reactions to proceed more readily, while cross-sensitivity to interfering gases was limited.

Acknowledgements

The authors thank Mr. Robert Novak and Dr. Jaco Visser at Ford Motor Company and Dr. Leta Woo at CoorsTek for the useful discussions and insight. The authors also thank Dr. Sven Eklund at Louisiana Tech University for providing additional laboratory resources. This study was supported through a project funded by the National Science Foundation under the Ceramics Division (DMR-1410670).

References

[1] L.P. Martin, L.Y. Woo, R.S. Glass, Impedancemetric NO_x Sensing Using YSZ Electrolyte and YSZ⁄Cr_2O_3 Composite Electrodes, J. Electrochem. Soc. 154 (2007) J97-J104. doi:10.1149/1.2430646.

[2] J.M. Rheaume, A.P. Pisano, Investigation of an impedancemetric NO_x sensor with gold wire working electrodes, J. Solid State Electrochem. 16 (2012) 3603–3610. doi:10.1007/s10008-012-1792-6.

[3] J. Fergus, Materials for high temperature electrochemical NO_x gas sensors, Sensors Actuators B Chem. 121 (2007) 652–663. doi:10.1016/j.snb.2006.04.077.

[4] T. Ueda, T. Nagano, H. Okawa, S. Takahashi, Zirconia-based amperometric sensor using La-Sr-based perovskite-type oxide sensing electrode for detection of NO_2, Electrochem. Commun. 11 (2009) 1654–1656. doi:10.1016/j.elecom.2009.06.030.

[5] L.Y. Woo, R.S. Glass, R.F. Novak, J.H. Visser, Effect of Electrode Material and Design on Sensitivity and Selectivity for High Temperature Impedancemetric NO_x Sensors, J. Electrochem. Soc. 157 (2010) J81-J87. doi:10.1149/1.3280263.

[6] J. Zou, X. Liu, H. Jin, Z. Zhan, J. Jian, NO_2 sensing properties of electrode-supported sensor by tape casting and co-firing method, Ionics. 21 (2015) 2655–2662. doi:10.1007/s11581-015-1430-2.

[7] T. Ueda, M. Umeda, H. Okawa, S. Takahashi, Effects of Sr Addition to La-Based Perovskite Sensing-Electrode on YSZ-Based Amperometric-Type NOx Sensor, IOP Conf. Ser. Mater. Sci. Eng. 18 (2011). doi:10.1088/1757-899X/18/21/212012.

[8] P.K. Sekhar, E.L. Brosha, R. Mukundan, M.A. Nelson, D. Toracco, F.H. Garzon, Effect of yttria-stabilized zirconia sintering temperature on mixed potential sensor performance, Solid State Ionics. 181 (2010) 947–953. doi:10.1016/j.ssi.2010.05.029.

[9] L.Y. Woo, L.P. Martin, R.S. Glass, W. Wang, S. Jung, R.J. Gorte, E.P. Murray, R.F. Novak, J.H. Visser, Effect of Electrode Composition and Microstructure on Impedancemetric Nitric Oxide Sensors Based on YSZ Electrolyte, J. Electrochem. Soc. 155 (2007) 32–40. doi:10.1149/1.2804766.

[10] L. Woo, R. Glass, NO_x sensor development, Lawrence Livermore National Laboratory Report (2010).

[11] N. Miura, T. Sato, S.A. Anggraini, H. Ikeda, S. Zhuiykov, A review of mixed-potential type zirconia-based gas sensors, Ionics (Kiel). 20 (2014) 901–925. doi:10.1007/s11581-014-1140-1.

[12] Y.X. Liu, J. Parisi, X.C. Sun, Y. Lei, Solid-state gas sensors for high temperature applications - a review, J. Mater. Chem. A. 2 (2014) 9919–9943. doi:10.1039/c3ta15008a.

[13] P. Elumalai, V. V. Plashnitsa, Y. Fujio, N. Miura, Highly sensitive and selective stabilized zirconia-based mixed-potential-type propene sensor using NiO/Au composite sensing-electrode, Sensors Actuators, B Chem. 144 (2010) 215–219. doi:10.1016/j.snb.2009.10.063.

[14] F. Sun, X. Li, L. Liu, J. Wang, Novel Zn–M–O (M=Sn, Co) sensing electrodes for selective mixed potential CO/C_3H_8 sensors, Sensors Actuators B Chem. 184 (2013) 220–

227. doi:10.1016/j.snb.2013.04.002.
[15] Y. Fujio, S.A. Anggraini, H. Ikeda, N. Terasaki, N. Miura, Improvement in Response/Recovery Characteristics of Mixed-Potential-Type Zirconia-Based CO Sensor Using $ZnCr_2O_4$ Added with Au Particles-Sensing Electrode, ECS Transactions. 75 (2016) 59–64.
[16] V. V. Plashnitsa, P. Elumalai, Y. Fujio, T. Kawaguchi, N. Miura, U. Guth, Spontaneous gradual accumulation of hexagonally-aligned nano-silica on gold nanoparticles embedded in stabilized zirconia: a pathway from catalytic to NH_3-sensing performance, Nanoscale. 3 (2011) 2286. doi:10.1039/c1nr10091b.
[17] U. Guth, J. Zosel, Electrochemical solid electrolyte gas sensors — hydrocarbon and NO_x analysis in exhaust gases, Ionics (Kiel). 10 (2004) 366–377. doi:10.1007/BF02377996.
[18] C. Yin, Y. Guan, Z. Zhu, X. Liang, B. Wang, Q. Diao, H. Zhang, J. Ma, F. Liu, Y. Sun, J. Zheng, G. Lu, Highly sensitive mixed-potential-type NO_2 sensor using porous double-layer YSZ substrate, Sensors Actuators, B Chem. 183 (2013) 474–477. doi:10.1016/j.snb.2013.03.064 Short communication.
[19] I. Romanytsia, J.-P. Viricelle, P. Vernoux, C. Pijolat, Application of advanced morphology Au–X (X=YSZ, ZrO_2) composites as sensing electrode for solid state mixed-potential exhaust NOx sensor, Sensors Actuators B Chem. 207 (2015) 391–397. doi:10.1016/j.snb.2014.10.017.
[20] S. Barison, M. Battagliarin, S. Daolio, M. Fabrizio, E. Miorin, P.L. Antonucci, S. Candamano, V. Modafferi, E.M. Bauer, C. Bellitto, G. Righini, Novel Au/$La_{1-x}Sr_xMnO_3$ and Au/$La_{1-x}Sr_xCrO_3$ composites: Catalytic activity for propane partial oxidation and reforming, Solid State Ionics. 177 (2007) 3473–3484. doi:10.1016/j.ssi.2006.10.005.
[21] P. Schmidt-zhang, Studies on the development of amperometric high temperature-NO-gas sensors on the basis of zirconium dioxide, Technical University of Berlin, Berlin, Germany, 2008.
[22] R.M.L. Werchmeister, K.K. Hansen, M. Mogensen, Characterization of $(La_{1-x}Sr_x)_sMnO_3$ and Doped Ceria Composite Electrodes in NOx-Containing Atmosphere with Impedance Spectroscopy, J. Electrochem. Soc. 157 (2010) P35–P42. doi:10.1149/1.3327892.
[23] T. Striker, V. Ramaswamy, E.N. Armstrong, P.D. Willson, E.D. Wachsman, J. a. Ruud, Effect of nanocomposite Au–YSZ electrodes on potentiometric sensor response to NOx and CO, Sensors Actuators B Chem. 181 (2013) 312–318. doi:10.1016/j.snb.2013.02.039.
[24] S.A. Anggraini, V. V. Plashnitsa, P. Elumalai, M. Breedon, N. Miura, Stabilized zirconia-based planar sensor using coupled oxide(+Au) electrodes for highly selective CO detection, Sensors Actuators, B Chem. 160 (2011) 1273–1281. doi:10.1016/j.snb.2011.09.062.
[25] N. Sakai, K. Yamaji, T. Horita, Y.P. Xiong, H. Kishimoto, M.E. Brito, H. Yokokawa, Effect of water on electrochemical oxygen reduction at the interface between fluorite-type oxide-ion conductors and various types of electrodes, Solid State Ionics. 174 (2004) 103–109. doi:10.1016/j.ssi.2004.07.027.
[26] L. Cui, F. Han, W. Dai, E.P. Murray, Influence of Microstructure on the Sensing Behavior of NO_x Exhaust Gas Sensors, J. Electrochem. Soc. 161 (2013) B34–B38. doi:10.1149/2.019403jes.
[27] M.C. Steil, F. Thevenot, Densification of Yttria-Stabilized Zirconia, J. Electrochem. Soc. 144 (1997) 390. doi:10.1149/1.1837416.
[28] S. Zhuiykov, N. Miura, Development of zirconia-based potentiometric NO_x sensors for

automotive and energy industries in the early 21st century: What are the prospects for sensors?, Sensors Actuators B Chem. 121 (2007) 639–651. doi:10.1016/j.snb.2006.03.044.

[29] K. A. Stoerzinger, W.T. Hong, G. Azimi, L. Giordano, Y.-L. Lee, E.J. Crumlin, M.D. Biegalski, H. Bluhm, K.K. Varanasi, Y. Shao-Horn, Reactivity of Perovskites with Water: Role of Hydroxylation in Wetting and Implications for Oxygen Electrocatalysis, J. Phys. Chem. C. (2015) 150715102419000. doi:10.1021/acs.jpcc.5b06621.

[30] D.T. Chaopradith, D.O. Scanlon, C.R.A. Catlow, Adsorption of Water on Yttria-Stabilized Zirconia, J. Phys. Chem. C. 119 (2015) 22526–22533. doi:10.1021/acs.jpcc.5b06825.

[31] L.Y. Woo, L.P. Martin, R.S. Glass, R.J. Gorte, Impedance Characterization of a Model Au/Yttria-Stabilized Zirconia/Au Electrochemical Cell in Varying Oxygen and NO_x Concentrations, J. Electrochem. Soc. 154 (2007) J129-J135. doi:10.1149/1.2456328.

[32] M. Stranzenbach, B. Saruhan, Planar , Impedancemetric NO_x Sensor with Spinel- type SE, Sensors Actuators B Chem. 127 (2007) 224–230.

[33] L.Y. Woo, R.S. Glass, R.F. Novak, J.H. Visser, Diesel engine dynamometer testing of impedancemetric NO_x sensors, Sensors Actuators B Chem. 157 (2011) 115–121. doi:10.1016/j.snb.2011.03.034.

[34] E. Koep, D.S. Mebane, R. Das, C. Compson, M.L. Liu, Characteristic thickness for a dense $La_{0.8}Sr_{0.2}MnO_3$ electrode, Electrochem. Solid State Lett. 8 (2005) A592–A595. doi:10.1149/1.2050607.

[35] G.J. la O', B. Yildiz, S. McEuen, Y. Shao-Horn, Probing Oxygen Reduction Reaction Kinetics of Sr-Doped $LaMnO_3$ Supported on Y_2O_3-Stabilized ZrO_2, J. Electrochem. Soc. 154 (2007) B427. doi:10.1149/1.2508887.

[36] E. Navickas, T.M. Huber, Y. Chen, W. Hetaba, G. Holzlechner, G. Rupp, M. Stöger-Pollach, G. Friedbacher, H. Hutter, B. Yildiz, J. Fleig, Fast oxygen exchange and diffusion kinetics of grain boundaries in Sr-doped $LaMnO_3$ thin films, Phys. Chem. Chem. Phys. 17 (2015) 7659–7669. doi:10.1039/C4CP05421K.

[37] Y. Takeda, Cathodic Polarization Phenomena of Perovskite Oxide Electrodes with Stabilized Zirconia, J. Electrochem. Soc. 134 (1987) 2656. doi:10.1149/1.2100267.

[38] L. Navarrete, C. Solis, and J.M. Serra, Boosting the oxygen reduction reaction mechanisms in IT-SOFC cathodes by catalytic fuctionalization, J. Mater. Chem A, 3 (2015) 16440-16444. doi: 10.1039/C5TA05187H.

Table 1. Power law exponent determined for sensors with different sensing electrodes evaluated with various gas concentrations of NO and H_2O at 575 °C.

Power Law Exponent, *m*				
Sensing Electrode	O_2 only	O_2 + 75 ppm NO	O_2 + 10% H_2O	O_2 + 75 ppm NO + 10% H_2O
LSM	-0.17	-0.13	-0.27	-0.24
LSM-Au	-0.24	-0.20	-0.26	-0.23
LSM-YSZ	-0.14	-0.12	-0.21	-0.20

Fig. 1. Schematic diagram of the NO_x gas sensor.

Fig. 2. SEM images of the surfaces of the (a) LSM pellet, (b) LSM-Au composite pellet (backscattered), (c) LSM-YSZ composite pellet, and (d) YSZ electrolyte.

Fig. 3. Typical impedance response of sensors with an (a) LSM, (b) LSM-Au, and (c) LSM-YSZ sensing electrode at 575 °C.

Fig. 4. Equivalent circuit for the NO_x sensors.

Fig. 5. Typical frequency response of sensors with an (a) LSM, (b) LSM-Au, and (c) LSM-YSZ sensing electrode at 575 °C.

Fig. 6. Comparison of the NO sensitivity of the LSM, LSM-Au and LSM-YSZ electrode based sensors at 575 °C for (a) dry (b) humidified conditions.

Fig. 7. Time based response of the NO_x sensors at an operating temperature of 575 °C.

Fig. 8. The selectivity of the LSM-Au based sensors is presented for NO, NO_2, CO, CO_2, and CH_4 with air as a background at an operating temperature of 575 °C.

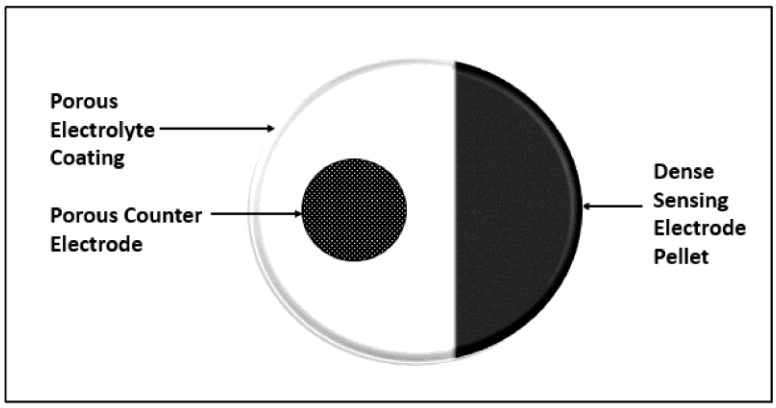

Fig. 1

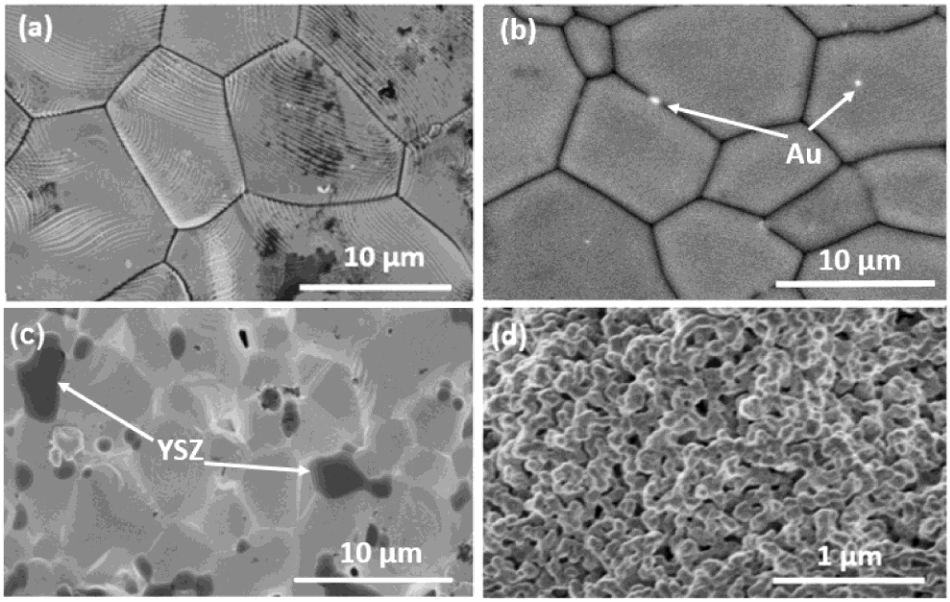

Fig. 2

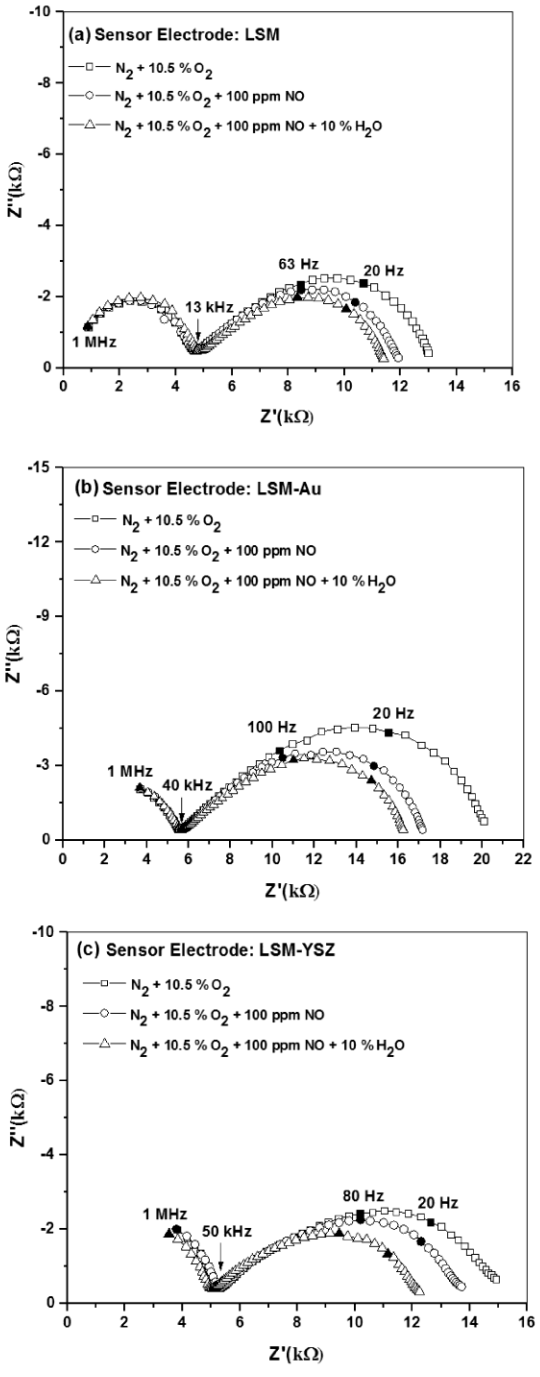

Fig. 3

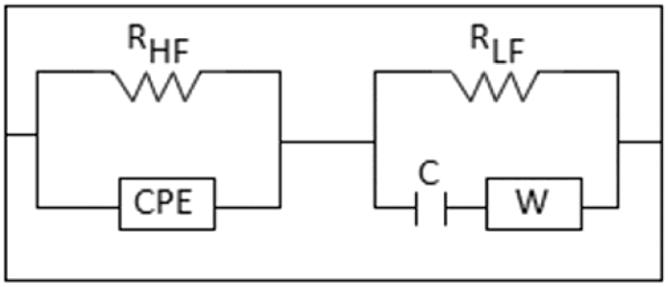

Fig. 4

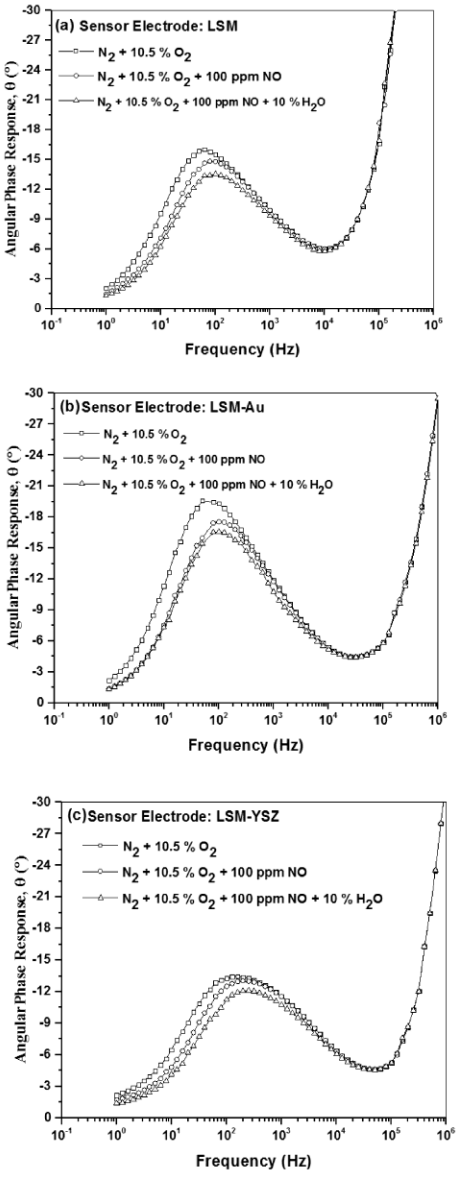

Fig. 5

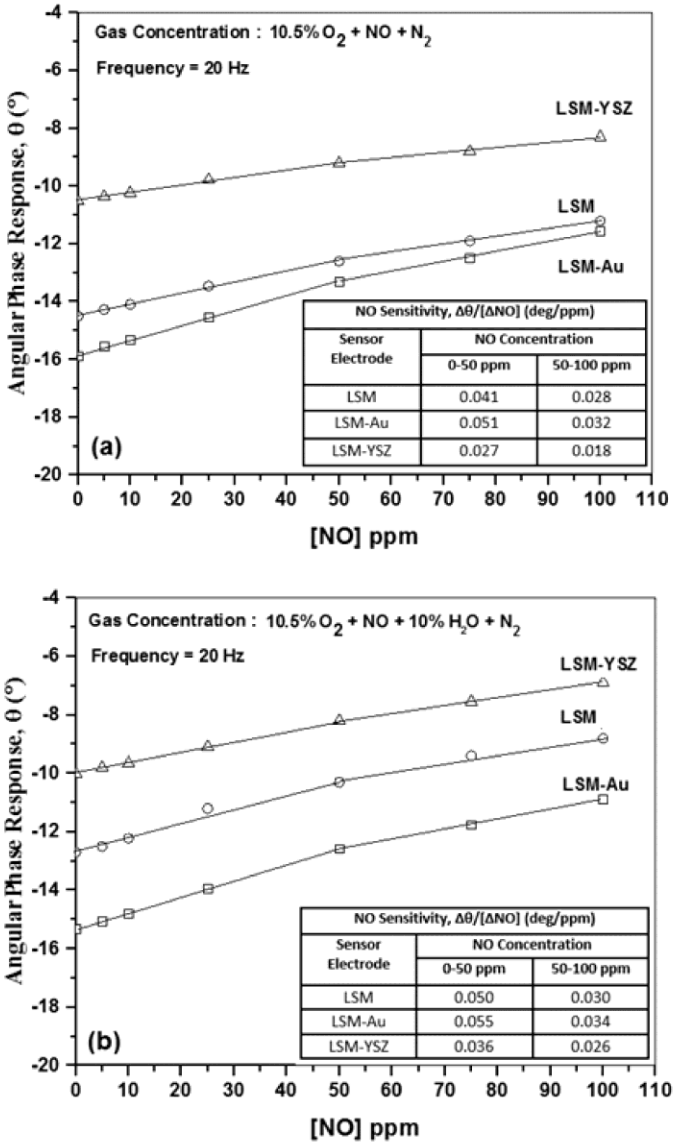

Fig. 6

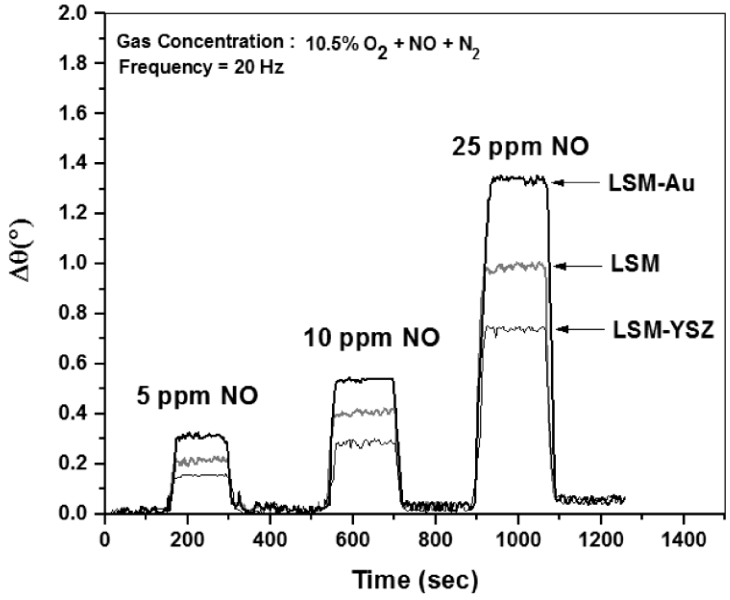

Fig. 7

Author Biographies

Dr. Nabamita Pal received her PhD degree in Micro and Nano Systems Engineering in 2017 from Louisiana Tech University, Ruston, Louisiana. Her research focused on NO_x sensors for diesel vehicle exhaust systems. She completed her M.S degree in Electrical Engineering from Louisiana Tech University in 2017; and has a B.Tech in Electrical Engineering from West Bengal University of Technology, India.

Dr. Erica Perry Murray received her PhD degree in Materials Science and Engineering from Northwestern University, Evanston, Illinois. She earned a BS in Physics from the University of California at San Diego in California. Presently, she is a Research Assistant Professor at the Institute for Micromanufacturing at Louisiana Tech University. Her research concerns electrochemical behavior of electroceramic materials.